Available online at www.sciencedirect.com
ScienceDirect
Polymer 48 (2007) 1083–1095
polymer
www.elsevier.com/locate/polymer

# Ubiquity of soft glassy dynamics in polypropylene–clay nanocomposites

Mark A. Treece, James P. Oberhauser*

*Department of Chemical Engineering, University of Virginia, 102 Engineer's Way, P.O. Box 400741, Charlottesville, VA 22904-4741, United States*

Received 25 August 2006; received in revised form 8 December 2006; accepted 15 December 2006
Available online 22 December 2006

**Abstract**

The rheology of polypropylene–clay nanocomposites was studied as a function of organoclay loading, degree of exfoliation, and presence of maleic anhydride functionalized polypropylene compatibilizer. Samples exhibit varying degrees of solid-like response in the terminal regime of small-amplitude oscillatory shear (SAOS), certifying that differences in clay silicate delamination were achieved for fixed organoclay loading. Previous work has also demonstrated that mechanically percolated nanocomposites exhibit logarithmically increasing storage modulus with time at low frequency, behavior attributed to the continuous development of a mesoscale organoclay network akin to that observed for colloidal gels. Continuous low frequency SAOS experiments not only affirm such behavior but also reveal that it is ubiquitous to polypropylene–clay nanocomposites, including samples whose organoclay loading and extent of exfoliation place them below the ostensible mechanical percolation threshold. Similar experiments conducted on uncompatibilized samples support the analogy to soft glassy dynamics, whereby van der Waals attractions drive the formation of a heterogeneous, gel-like organoclay network. Intermolecular associations between pendant group functionalities on the compatibilizer have contributed to logarithmic increases in the storage modulus with time for pure maleated samples, but the reduced concentrations of maleated polypropylene present in the materials reported here are shown to not influence the solid-like rheology over time through network formation. Thus, we demonstrate that only organoclay network formation is responsible for the time-dependent rheology in polyolefin nanocomposites.
Published by Elsevier Ltd.

*Keywords:* Nanocomposites; Rheology; Colloidal gel

## 1. Introduction

For more than a decade, polymer–clay nanocomposites (PCNs) have been the subject of intense research interest stimulated by significant improvements in solid-state mechanical, thermal, dimensional, and barrier properties at volume fractions much less than those employed for conventional microscale fillers [1–6]. Montmorillonite (MMT), which belongs to the 2:1 phyllosilicate structural family, is perhaps the most frequently used nanofiller. Its ability to improve material properties is predicated upon its large surface area (ca. 750 $m^2/g$) [7], small clay silicate thickness (ca. 1 nm) [8], and large aspect ratio for an individual platelet (ca. 400–1000 nm) [9]. To capitalize upon these geometric properties, however, a favorable thermodynamic interaction between the clay and matrix polymer is critical. That objective is rendered more challenging by the fact that individual clay silicate layers naturally form tactoid domains comprising numerous platelets separated by a charged intergallery, which precludes exfoliation of individual platelets in hydrophobic polymers. As a result, it is customary to perform a cation exchange reaction using alkylammonium surfactants to make the clay silicate surfaces organophilic, improve miscibility, and expand the intergallery region between individual layers [10]. Importantly, the swelling of the intergallery reduces the entropic penalty for macromolecules to diffuse into that region, expanding the intergallery further and increasing the likelihood of delamination of platelets.

However, clay surface modification is insufficient to alter the negative enthalpic interaction between organically modified clay (or organoclay) and highly nonpolar polymers (e.g., polyethylene, polypropylene). Consequently, macromolecules

* Corresponding author. Tel.: +1 434 924 7974; fax: +1 434 982 2658.
*E-mail address:* oberhauser@virginia.edu (J.P. Oberhauser).

0032-3861/$ - see front matter Published by Elsevier Ltd.
doi:10.1016/j.polymer.2006.12.029

of those chemistries remain thermodynamically prohibited from diffusing into intergalleries. To improve compatibility between nonpolar polymers and organoclay, a low molecular weight copolymer of the matrix polymer and maleic anhydride is frequently added as a compatibilizer. The compatibilizer, referred to as PP-*g*-MA in the case of polypropylene, interacts with the organoclay through hydrogen bonding between the polar succinic anhydride groups and the oxygen groups on the clay silicates [11]. Significant work has been done in studying the influence of compatibilizer loading on organoclay exfoliation and dispersion, and results suggest that efficacy saturates beyond a 3:1 mass ratio of PP-*g*-MA to organoclay [12–16].

Several experimental techniques have been employed to characterize the structure of PCNs at a variety of length scales. X-ray diffraction (XRD) and transmission electron microscopy (TEM) are among the most common. The small wavelength of the incident X-ray beam makes XRD effective at probing the $O$(nm) length scale associated with the basal ($d_{001}$) spacing in a tactoid domain. However, XRD is vulnerable to signal-to-noise problems in materials with low filler content [17,18] and reliant upon an isotropic distribution of organoclay domain orientation states, making the preparation of samples for XRD experiments an important consideration [19,20]. Therefore, while it can determine the mean basal spacing, XRD cannot provide quantitative information about the mean number of platelets per tactoid or independently affirm clay exfoliation [21,22]. By imaging on the $O$(10–100 nm) length scale, TEM is better able to qualitatively assess the state of exfoliation in PCNs; however, it is very difficult to quantify subtle differences in exfoliation and dispersion from TEM images due in part to variability in those characteristics across the sample. Moreover, both XRD and TEM are solid-state measurements, offering only an instantaneous picture of local structure but no sense of how the mesoscale structure may evolve over time.

Rheology has proven to be exquisitely sensitive to particle loading, shape, size, and distribution for a wide range of filler types [23]. A range of linear and nonlinear deformation histories have been applied to a broad spectrum of PCN chemistries, including polypropylene (PP) [16,24–31], polyethylene (PE) [32–35], nylon-6 [36,37], polystyrene (PS) [38–42], poly($\varepsilon$-caprolactone) [8,36,43], polystyrene–polyisoprene (PS–PI) block copolymers [44–46], and poly(isobutylene-*co*-*p*-methylstyrene) (PIB–PS) block copolymers [41]. The terminal behavior during small-amplitude oscillatory shear (SAOS) has drawn particular interest due to the observed transition from liquid-like ($G' \propto \omega^2$, $G'' \propto \omega$) to solid-like ($G'$, $G'' \propto \omega^0$) rheology ascribed to the formation of a volume-spanning, mesoscale organoclay network above the mechanical percolation threshold [24,25,28,29,31,41,47]. XRD and TEM cannot elucidate structure on the length scales germane to networking behavior.

Additionally, intriguing time-dependent terminal rheology has been reported for polymers with varying hydrophobic character. Organoclay disorientation kinetics of PIB–PS and PS nanocomposites following large-amplitude oscillatory shear (LAOS) alignment were studied by Ren et al., who noted a modest logarithmic *increase* in the terminal storage modulus with annealing time over several hours [41]. The effect was observed to be independent of the molecular weight and viscosity of the matrix polymer and type of organoclay. Importantly, the polymers chosen for the study did not require compatibilization. Galgali et al. examined the linear viscoelastic rheology of PP–clay nanocomposites in the presence and absence of PP-*g*-MA compatibilizer [25]. Sequential SAOS frequency sweeps were performed on samples not subjected to pre-shear, and consistent *decreases* in both storage and loss moduli with annealing time were reported for a 2.5 h period. However, subsequent creep experiments show a continuously increasing zero-shear viscosity with annealing time for both compatibilized and uncompatibilized blends, a result that is seemingly at odds with the SAOS data. To address inconsistency in the Galgali et al. data, Treece and Oberhauser recently presented results for a 3 wt% compatibilized PP–clay nanocomposite subjected to a battery of linear and nonlinear rheological tests [31]. Both unsheared and pre-sheared samples exhibited a logarithmic *increase* in storage modulus with annealing time over several hours. Moreover, the logarithmic increase occurred at two different rates, a weak dependence for approximately the first 3 h akin to that reported by Ren et al. followed by a stronger dependence at longer annealing times. In all samples, the increases in storage modulus could be erased by subsequent shearing and the process begun anew, highlighting the reversibility of the network formation process.

The aforementioned rheological phenomenon has been explained in terms of time-dependent changes in mesoscale organoclay structure and a compelling analogy drawn to the dynamics of soft colloidal glasses [31,41]. Aqueous Laponite clay dispersions, soft colloidal pastes, and particulate gels have all been classified as soft colloidal glasses in that they exhibit yield behavior, thixotropy, and slow recovery following a deformation [48–54]. Since these properties often evolve continuously with time, these soft glassy dynamics are frequently described as "aging" phenomena and associated with metastable, structural heterogeneity on microscopic to mesoscopic length scales [55–57]. For example, the storage modulus and complex viscosity of aqueous Laponite dispersions have shown logarithmic dependence on time like that described for PCNs. In the case of the dispersions, the structural rearrangements responsible for the rheological behavior depend upon the ionic strength of the dispersion, which tunes the balance of attractive and repulsive forces between clay domains. A dispersion with low ionic strength, often referred to as a glass, is characterized by long-range electrostatic repulsion and short-range attraction that lead to a homogeneous structure on interparticle distances with elasticity derived from caging effects [58–60]. By contrast, high ionic strength screens long-range repulsive forces, creating a gel with a percolated, heterogeneous, infinite network [61]. With long-range repulsive interactions negated by the surfactant modifier in these PCNs, short-range van der Waals attractions are the principle driving force for microstructural change in these materials, making them similar to attractive colloidal gels [24,31].

In the case of PP–clay nanocomposites, it is possible that the PP-*g*-MA compatibilizer also contributes to a time-dependent increase in dynamic moduli in nanocomposites based on polyolefins. Lee et al. performed low frequency SAOS experiments on pure maleated polyethylene (PE-*g*-MA) and observed significant logarithmic increases in storage and loss moduli over a period of 1 h [32]. Their results strongly point to dipole–dipole and hydrogen-bonding interactions between pendant succinic anhydride and succinic acid functionalities, the latter formed through the hydrolysis of succinic anhydride [62] and driving the formation of a reversible, labile network. Similar pendant group associations for PP-*g*-MA are possible, although it remains unclear whether they are present at the reduced concentration of compatibilized PP–clay nanocomposites or are otherwise disrupted by the presence of organoclay.

In this work, the objective is to examine the influence of organoclay loading, extent of exfoliation, and compatibilizer on the rheology ascribed to soft glassy dynamics in PP–clay nanocomposites. Samples containing 1, 3, and 5 wt% organoclay were melt-blended using processes known to impart different degrees of exfoliation and dispersion [19]. By varying organoclay loading and degree of exfoliation, we are able to determine if mechanical percolation is a necessary condition for the development of solid-like rheology or if, like colloidal gels, a volume-spanning network driven by attractive forces can form at loadings otherwise associated with liquid-like rheology. Finally, uncompatibilized samples at the three organoclay loadings and one blend of PP and PP-*g*-MA were also prepared in order to elucidate the independent contributions of organoclay and compatibilizer to the long-time rheological behavior.

## 2. Experimental

### 2.1. Materials

Polypropylene (PP, Dow Chemical grade H700-12, MFI = 12 g/10 min at 230 °C and 2.16 kg load, $M_w$ = 229,000 g/mol, $M_w/M_n = 3.98$) containing standard antioxidant additives was used as-received as the matrix polymer. Southern Clay Products provided Cloisite® 15A (C15A, 125 meq/100 g, $d_{001} = 31.5$ Å), a natural MMT clay modified with a ditallow quaternary ammonium salt (2M2HT). Polybond® 3200 (PP-*g*-MA, Crompton Corp., MFI = 110 g/10 min at 190 °C and 2.16 kg load), a 1 wt% maleic anhydride functionalized polypropylene, was used as the compatibilizer.

Nanocomposites containing 1, 3, and 5 wt% C15A were prepared in one of three ways. The first set of samples was melt-blended using a masterbatch (MB) approach in which PP-*g*-MA and C15A were initially processed in a Leistritz Micro 27 twin-screw extruder ($L/D = 52$, $D = 27$ mm) operating with co-rotating screws (200–210 °C, 200 rpm). PP-*g*-MA was metered to the screws at a rate of 5 lb/h, and C15A was concurrently added via a side-stuffer located halfway down the barrel (26D) at a rate required to obtain a 3:1 ratio of PP-*g*-MA to C15A. The selection of the 3:1 ratio was predicated on reports of other researchers, who noted that continued improvement in exfoliation and dispersion was no longer observed above that level [12,13,16]. In the second dilution processing step, MB material was dry mixed with appropriate amounts of PP and metered to counter-rotating screws (190 °C, 300 rpm) at a rate of 20 lb/h. Both MB and final products were extruded into a water bath, pelletized, and oven dried at 80 °C for 12 h prior to the dilution step or subsequent characterization. Hereafter, we will refer to these samples prepared in the twin-screw extruder as "TSE" blends.

The second set of samples was processed identically to the TSE samples but in the absence of PP-*g*-MA. Hence, in the MB step, PP was substituted for compatibilizer. The resulting MB was then further diluted with PP in the manner described previously for the second extrusion step. In all other ways, these "TSE (no PP-*g*-MA)" blends were prepared identically to the TSE materials.

The third set of nanocomposites was prepared in a single-screw extruder (Killion, $L/D = 24$, $D = 25.4$ mm) equipped for direct addition of supercritical carbon dioxide (*sc*$CO_2$). A MuCell® supercritical fluid system (Trexel Inc.) delivered *sc*$CO_2$ to the screws two-thirds of the way down the barrel length. The density of *sc*$CO_2$ leaving the chiller was 843.2 kg/m$^3$, and the flow rate was set to 5% of the extrusion rate to match the maximum absorption capacity of $CO_2$ in PP [63]. Material was processed twice with barrel temperatures set at 190–210 °C and a screw speed of 15 rpm. The second pass was conducted without *sc*$CO_2$ addition to improve mixing of the nanocomposite and remove foam generated by the first *sc*$CO_2$ pass. A more comprehensive description of material properties for these "*sc*$CO_2$" blends is available elsewhere [19].

Control samples of matrix PP and PP with 9 wt% PP-*g*-MA were processed in a single pass in the Leistritz twin-screw extruder with co-rotating screws at 200–210 °C and 200 rpm. The processed PP sample will simply be referred to as "PP", while the compatibilized polymer will be named "PP/9 wt% PP-*g*-MA." Because the latter sample has identical compatibilizer content to the 3 wt% TSE and *sc*$CO_2$ samples, its results may be contrasted with those samples to separate the influences of compatibilizer and clay on long-time rheological behavior.

### 2.2. X-ray diffraction

XRD was conducted in reflection mode on 1.5 mm thick compression molded nanocomposite samples using a Scintag XDS 2000 diffractometer ($CuK_\alpha$ radiation source, $\lambda = 1.541$ Å). Data were acquired with a step size of 0.02° and a scan rate of 0.5°/min. The results presented are the average of two to four scans. The mean basal spacing of the organoclay was computed from Bragg's law and the angle corresponding to the primary diffraction peak.

### 2.3. Rheology

All rheological experiments were performed with a TA Instruments AR 2000 rheometer equipped with a 25 mm parallel

plate geometry and environmental test chamber (ETC). A nitrogen purge of 10 L/min was continuously supplied to the ETC to inhibit oxidative degradation of the PP during experiments. Compression molded samples (190 °C for 10 min) were melted at 210 °C for 10 min in the rheometer before the upper plate was lowered to a gap distance of 1 mm for testing.

Because SAOS has proven to be exceptionally sensitive to clay loading, degree of exfoliation, and dispersion of organoclay domains in polymeric liquids, two types of SAOS experiments were used to probe for solid-like behavior. First, traditional SAOS frequency sweeps have previously revealed a solid-like plateau in the storage modulus in the terminal (low frequency) regime, a response that has been ascribed to a volume-spanning, mesoscale organoclay network forming at loadings above that required for mechanical percolation [24,29,42,47]. Here, frequency sweeps were performed at 1% strain from high to low frequency in sequential steps at 210 °C, 180 °C, and 150 °C. Time–temperature superposition (TTS) was applied to shift data to a reference temperature of 180 °C. Since time-dependent changes in the terminal response may signal a shift in the mesoscale arrangement of organoclay domains, SAOS experiments at a fixed frequency of 0.01 Hz, 200 °C, and 1% strain were performed over a period of 11 h. In both types of experiments, the time-dependent rheological properties are best reflected through the storage modulus ($G'$), loss tangent ($\tan\delta \equiv G''/G'$), and complex viscosity ($|\eta^*|$), as the loss modulus ($G''$) is often only weakly affected by the presence of the organoclay.

## 3. Results and discussion

### 3.1. X-ray diffraction

XRD scans of the nine nanocomposite samples as well as as-received C15A are shown in Fig. 1. The vertical line passing through the primary C15A peak serves as a benchmark for whether the processing of the nanocomposites led to an increase or decrease in basal spacing relative to the dry organoclay. Qualitatively, the *sc*$CO_2$ and TSE blends have $d_{001}$ spacings comparable to that of C15A, except for the 5 wt% *sc*$CO_2$ sample that shows a modest shift to higher diffraction angle and therefore smaller intergallery distance. By contrast, the materials without PP-*g*-MA are uniformly shifted to higher angles (smaller spacings). This observation is quantitatively confirmed in Table 1, which details the peak location and associated basal spacing for each blend. As expected, the uncompatibilized materials at all organoclay loadings have smaller intergallery distances relative to the dry C15A and other nanocomposites. This reduction likely stems from degradation of surfactant, which has been shown to occur above 200 °C [64,65]. Because intercalation of PP between silicate layers is thermodynamically unfavorable, thermal degradation of the organic modifier during processing causes the intergallery spacing to decrease in the TSE (no PP-*g*-MA) blends. On the other hand, by virtue of its polarity and smaller molecular weight, diffusion of PP-*g*-MA between silicate layers is thermodynamically favorable; consequently, PP-*g*-MA intercalation may compensate for thermal degradation of surfactant in both *sc*$CO_2$ and TSE materials.

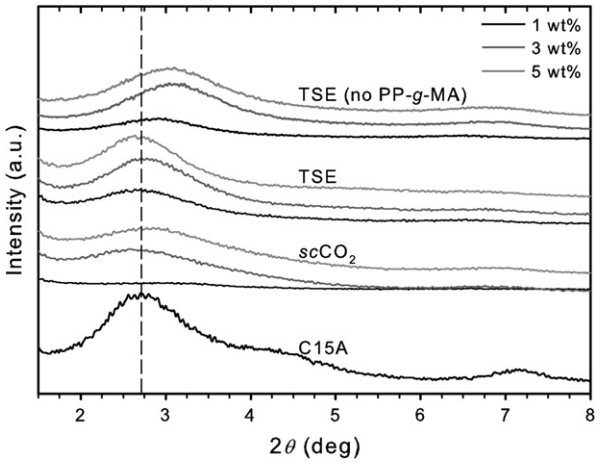


Fig. 1. XRD scans for compression molded 1, 3, and 5 wt% *sc*$CO_2$, TSE, and TSE (no PP-*g*-MA) nanocomposites compared with that for dry C15A clay.

The differences in the magnitude of the XRD peak intensities in Fig. 1 merit further discussion. For example, the *sc*$CO_2$ blends at any given organoclay loading appear to have smaller peak intensities than the comparable TSE and TSE (no PP-*g*-MA) samples, a feature that is often construed as evidence of superior exfoliation. However, TEM images and rheological data for the *sc*$CO_2$ blends presented elsewhere show that they are, in fact, quite poorly exfoliated [19]. We suspect that sample preparation plays an important role in the suppression of the *sc*$CO_2$ diffraction peak. Like other published work, the XRD samples were compression molded to a desired thickness and thus subjected to a modest squeezing flow, which may have altered the orientation distribution of the anisotropic organoclay domains. Since flow-induced orientation of organoclay domains should occur more readily for higher aspect ratio organoclay domains, better exfoliated materials (i.e., those with the fewest number of silicate layers per domain) should be most readily aligned in the flow direction. Presumably, if compression molded samples were allowed to anneal, flow-aligned organoclay domains would tend to disorient with time to some degree. Because the disorientation is a random process, it stands to reason that a significant number of domains that originally contributed to the diffraction intensity would rotate out-of-plane relative to the incident X-ray beam and no longer do so.

To explore this hypothesis, all nanocomposite materials were compression molded and subsequently annealed in the mold at 210 °C for 11 h in a vacuum oven. The XRD scans of 5 wt% annealed samples presented in Fig. 2 are representative of the other two organoclay loadings. The results are consistent with the above hypothesis, as the diffraction peaks of all three samples are significantly suppressed after annealing. In fact, in the case of the 5 wt% TSE blend, the peak has effectively vanished. It is critical to stress that we believe the diminution of the peaks in the annealed samples stems from

Table 1
Basal spacings inferred from XRD scans of dry C15A organoclay and 1, 3, and 5 wt% *sc*$CO_2$, TSE, and TSE (no PP-*g*-MA) nanocomposites

| | C15A | *sc*$CO_2$ | | | TSE | | | TSE (no PP-*g*-MA) | | |
|---|---|---|---|---|---|---|---|---|---|---|
| | | 1 wt% | 3 wt% | 5 wt% | 1 wt% | 3 wt% | 5 wt% | 1 wt% | 3 wt% | 5 wt% |
| Peak location ($2\theta$) | 2.71° | 2.725° | 2.72° | 2.825° | 2.76° | 2.737° | 2.70° | 3.10° | 3.12° | 3.04° |
| $d_{001}$ spacing (nm) | 3.257 | 3.239 | 3.245 | 3.125 | 3.198 | 3.225 | 3.269 | 2.848 | 2.829 | 2.904 |

organoclay disorientation relative to the incident X-ray beam and not further exfoliation of clay silicates. In addition to demonstrating the influence of sample preparation in XRD data, these results emphasize that XRD only provides quantitative information about the mean basal spacing and cannot be used to describe degree of exfoliation, tactoid size, or dispersion of organoclay domains. As a tool ubiquitously employed to characterize PCNs, XRD must be used cautiously and its results not overzealously interpreted.

### 3.2. SAOS frequency sweeps

Previous work with these materials indicated that processing history and formulation have imbued them with decidedly different exfoliation and dispersion characteristics [19,20]. SAOS oscillatory shear is effective at illustrating these differences, as the terminal response of the fluids is affected by the relative importance of clay–clay interactions. Fig. 3 presents TTS results for SAOS frequency sweeps of the 1, 3, and 5 wt% TSE blends as well as the processed PP control sample. It is immediately clear that the 1 wt% nanocomposite is virtually indistinguishable from PP except for a slight reduction in complex viscosity at low frequency. Since the nanocomposites are processed twice and PP once, it is likely that more significant thermomechanical degradation of the matrix PP occurs in the nanocomposite sample, causing a larger decrease in viscosity relative to PP processed in a single pass [66–69]. In terms of solid-like rheological behavior, however, the two samples are quite similar. By contrast, the 3 and 5 wt% TSE blends exhibit

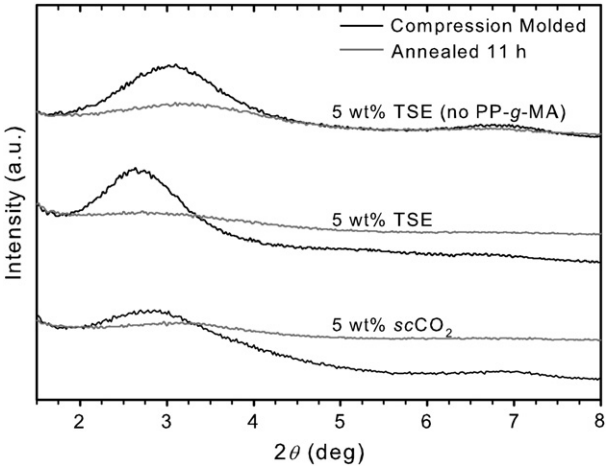


Fig. 2. XRD scans for 5 wt% *sc*$CO_2$, TSE, and TSE (no PP-*g*-MA) nanocomposites following compression molding (see Fig. 1) and also subsequent annealing at 210 °C in a vacuum oven for 11 h.

a number of rheological signatures indicative of a solid-like terminal response, including: (1) flattening of the slope of the storage modulus and increasing plateau values with increased loading; (2) a maximum in the loss tangent, denoting a transition to *decreasing* values with decreasing frequency; and (3) diverging complex viscosity, which is characteristic of materials with a yield stress. All of these attributes have been observed for other PCNs as well as polymeric fluids containing conventional fillers and highlight the increasing importance of particle–particle interactions in dictating the rheological response [24–26,28,29,36,41,47,70–74]. The transition in behavior observed between 1 and 3 wt% loadings is customarily ascribed to mechanical percolation, or the loading at which the filler particles form a volume-spanning network capable of bearing load. Below percolation, the filler increases the bulk viscosity due to hydrodynamic effects prevalent in all dilute suspensions.

Importantly, the organoclay loading at which mechanical percolation occurs depends strongly on the degree of exfoliation and dispersion in PCNs, since the number of organoclay domains is directly related to the extent to which silicate layers have been exfoliated. Hence, in a poorly exfoliated blend, individual organoclay domains will be larger and have greater distance between them; consequently, clay–clay interactions will be reduced relative to a better exfoliated sample of the same loading, and the rheology will more closely resemble that of the matrix polymer. The frequency sweep data for the *sc*$CO_2$ blends presented in Fig. 4 clearly demonstrate this fact. The storage modulus of the 1 and 3 wt% *sc*$CO_2$ materials shows small departures from PP at low frequency, but the most significant increase is observed at 5 wt%, although even this increase is dwarfed by those seen for the 3 and 5 wt% TSE samples. The terminal behavior of the loss tangent casts the three nanocomposite samples in sharper relief, as only the 5 wt% blend exhibits a maximum and subsequent downturn in loss tangent with decreasing frequency. Additionally, the 5 wt% sample is also the only one of this set to show a diverging complex viscosity. As a result, it is natural to conclude that mechanical percolation for these samples occurs between 3 and 5 wt%.

Two other features of Fig. 4 bear further mention. First, all three *sc*$CO_2$ nanocomposites have a larger low frequency complex viscosity than the processed PP in contrast to the result in Fig. 3 for the 1 wt% TSE and PP samples. Thus, it is clear that thermomechanical degradation is much less significant in the single-screw extruder used to prepare the *sc*$CO_2$ materials, to be expected given the lower rotation speed at which it was operated and known differences in applied stress relative to twin-screw extrusion. More intriguing is the apparent failure

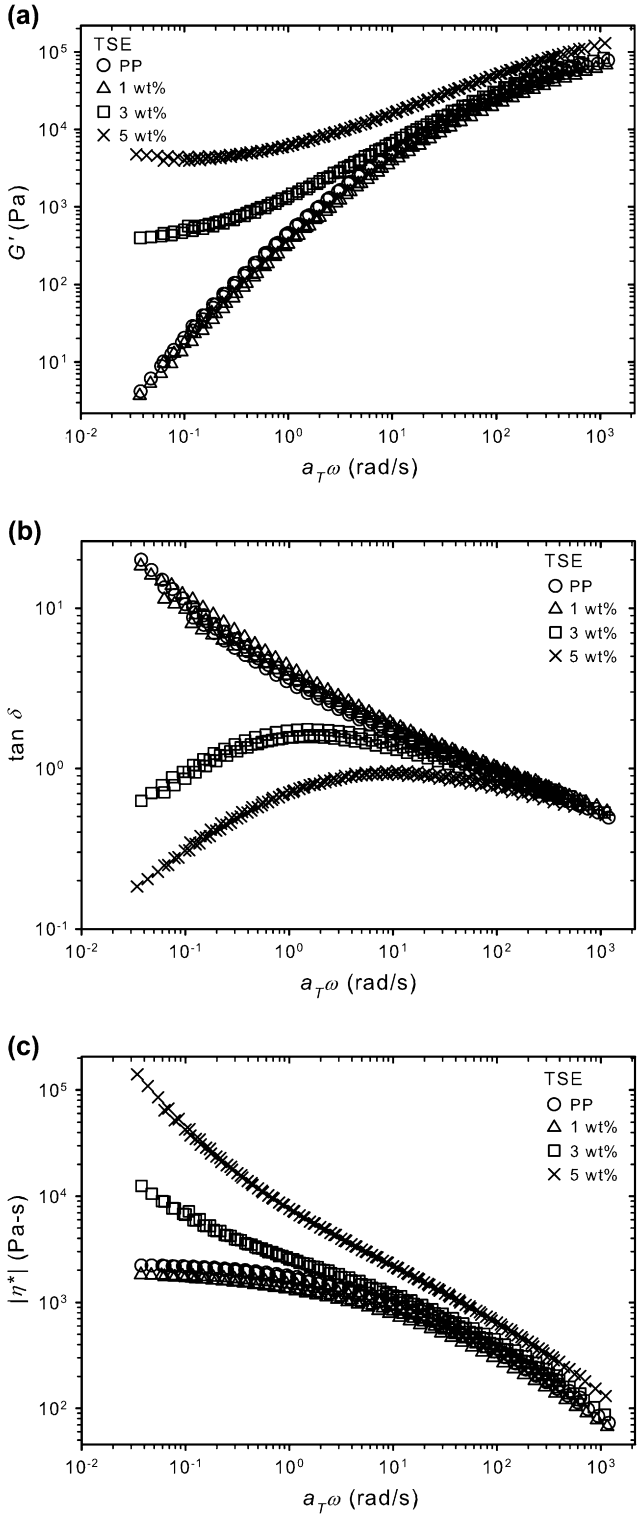


Fig. 3. SAOS frequency sweeps of 1, 3, and 5 wt% TSE blends and processed PP performed sequentially at 210 °C, 180 °C, and 150 °C at 1% strain. Time–temperature superposition was applied to shift data to 180 °C.

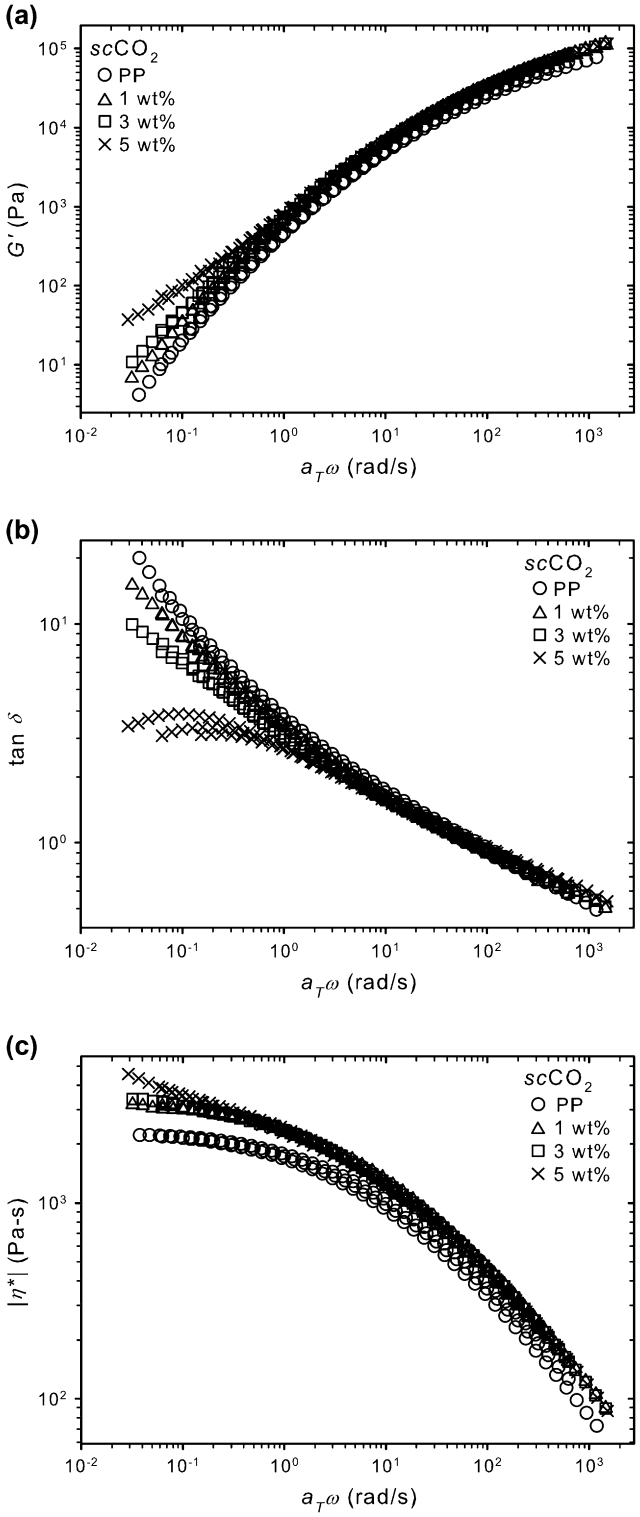


Fig. 4. SAOS frequency sweeps of 1, 3, and 5 wt% $sc$CO$_2$ blends and processed PP performed sequentially at 210 °C, 180 °C, and 150 °C at 1% strain. Time–temperature superposition was applied to shift data to 180 °C.

of TTS at low frequencies for the 5 wt% $sc$CO$_2$ sample, which is particularly evident from the results of the loss tangent. We recall that the frequency sweep experiments were performed sequentially at 210 °C, 180 °C, and 150 °C, where higher temperature sweeps access lower frequencies after shifting. Thus, it appears that the maximum in the loss tangent shifts to higher reduced frequency and decreases in value over the course of the three frequency sweeps. Similar behavior is seen to a lesser degree for the 3 wt% $sc$CO$_2$, 3 wt% TSE, and 5 wt% TSE blends. The underlying question is whether the effect stems

from thermal effects or time-dependent changes in the mesoscale distribution of organoclay domains. However, the quiescent crystallization time at 150 °C is several hours and much longer than the time scale for frequency sweep experiments conducted below the nominal melting point. Consequently, we believe that the failure of TTS in the terminal regime is a manifestation of mesoscale organoclay structural changes rather than crystallization or other thermal effects.

The results for the 1, 3, and 5 wt% TSE (no PP-*g*-MA samples) shown in Fig. 5 indicate a state of exfoliation and dispersion intermediate to the *sc*$CO_2$ and TSE blends. The 3 and 5 wt% TSE (no PP-*g*-MA) samples both exhibit a flattening of the storage modulus, maxima in the loss tangent, and divergent complex viscosity in the terminal regime, suggesting that mechanical percolation occurs between 1 and 3 wt% as in the TSE blends. However, the degree to which solid-like behavior manifests itself in the TSE (no PP-*g*-MA) materials is considerably less than the comparable TSE blends, reflecting the expected influence of compatibilizer on exfoliation and dispersion. The comparison with the *sc*$CO_2$ samples, on the other hand, emphasizes the importance of stress in mediating exfoliation and dispersion, as the inclusion of compatibilizer fails to engender significant exfoliation in the *sc*$CO_2$ blends prepared in the lower stress single-screw extruder. We again note a shifting in the loss tangent data for the 3 and 5 wt% TSE (no PP-*g*-MA) blends over the course of the three frequency sweeps, behavior that will be further explored in the subsequent section concerning the long-time terminal rheology of these materials.

Finally, we note that TEM images of all TSE and *sc*$CO_2$ samples have already been published [19]. These images reinforce the conclusions drawn from the rheological data, specifically that exfoliation and dispersion in the TSE samples are superior. Similar images for the TSE (no PP-*g*-MA) blends have not been included here, because one cannot qualitatively distinguish those samples from the other two sets. Moreover, the presentation of TEM images is inherently subjective, as any given image may not be representative of the entire sample. Therefore, the previous XRD data represent the sole measure of structure at the length scale of individual tactoids in this paper. We maintain that the larger length scale associated with the formation of a mesoscale particulate network, the focus of this work, is best probed by rheology.

### 3.3. SAOS long-time behavior

Work in our laboratory and those of other researchers suggests that the previously described shifts in the terminal loss tangent are likely due to time-dependent changes in the mesoscale distribution of organoclay domains [25,31,41]. For example, we recall that Ren et al. observed that the storage modulus of pre-sheared samples *increased* logarithmically with time ($G' \propto t^{\beta}$), where the exponent $\beta$ varied between 0.1 and 0.25 [41]. Meanwhile, conducting SAOS frequency sweeps on as-processed material annealed for up to 150 min, Galgali et al. reported a *decrease* in both storage and loss moduli for compatibilized and uncompatibilized blends [25].

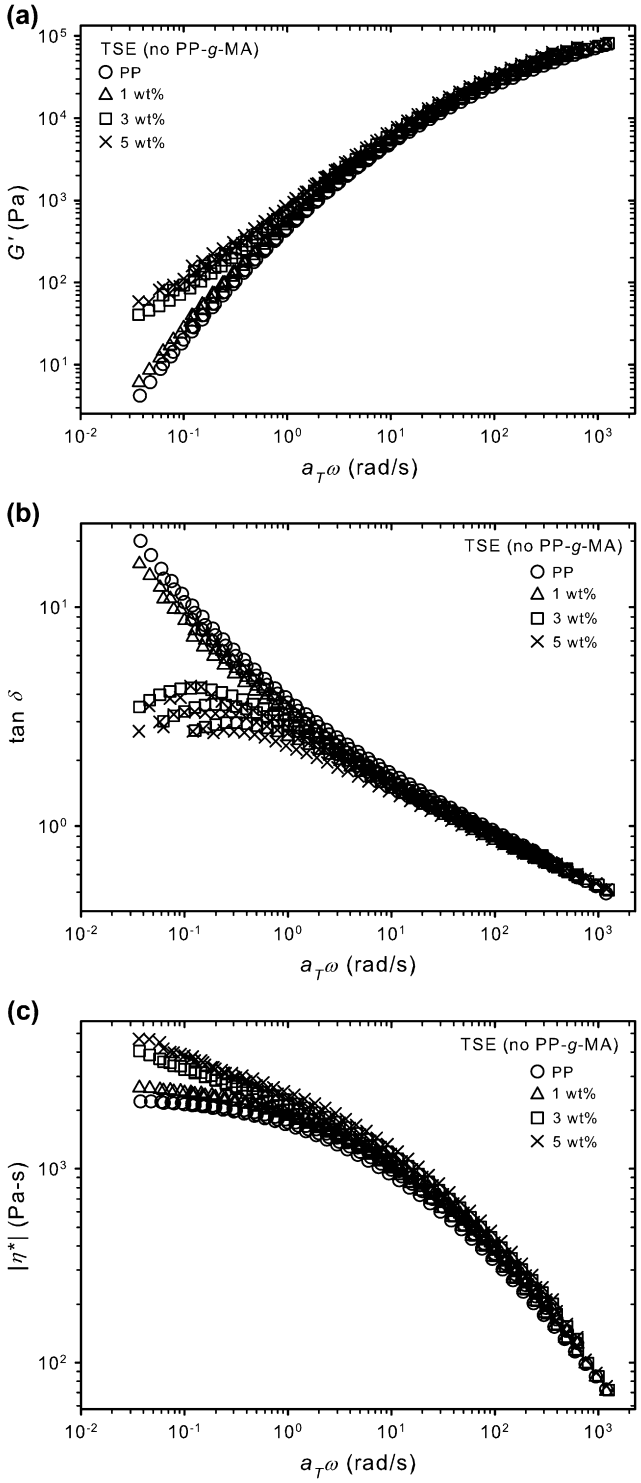


Fig. 5. SAOS frequency sweeps of 1, 3, and 5 wt% TSE (no PP-*g*-MA) blends and processed PP performed sequentially at 210 °C, 180 °C, and 150 °C at 1% strain. Time–temperature superposition was applied to shift data to 180 °C.

Finally, using long-time SAOS, Treece and Oberhauser described logarithmic dependence similar to that seen by Ren et al. for a different as-processed and pre-sheared 3 wt% compatibilized nanocomposite, although they noted an increase in the value of the exponent after long annealing times [31]. The conflicting results emphasize the need to further examine the

influence of organoclay loading, exfoliation, and dispersion on the phenomenon.

Therefore, we next report data for SAOS performed at fixed frequency (0.01 Hz) and temperature (200 °C) over a period of 11 h. Results for the 1, 3, and 5 wt% TSE blends are contrasted with those for processed PP in Fig. 6. Examining the data for PP first, we see that the storage modulus and complex viscosity decrease slowly over time while the loss tangent increases, responses that are consistent with thermal degradation of the matrix PP. We also point out that the loss modulus (data not shown) of PP also decreases with time, although to a lesser degree than the storage modulus as evidenced by the increase in loss tangent. Turning to the nanocomposites, entirely different long-time behavior is witnessed, as the storage modulus increases for all three organoclay loadings. For the 5 wt% TSE sample, it shows a consistently small logarithmic dependence ($\beta = 0.15$) akin to that observed by Ren et al., while the 3 wt% TSE blend exhibits the beginnings of the two-stage logarithmic increase seen by Treece and Oberhauser ($\beta = 0.17$ and $\beta = 0.46$). Intriguingly, the storage modulus of the 1 wt% TSE sample also shows clear two-stage logarithmic time-dependence ($\beta = 0.086$ and $\beta = 0.78$) despite the fact that its rheology in Fig. 3 was distinctly polymer-like. In a broader sense, the results in Fig. 6(a) call into question those of Galgali et al., since these compatibilized blends clearly show an *increase* in storage modulus with time. While we cannot explain the results of Galgali et al., we are confident that the results presented here are universal for PP–clay nanocomposites.

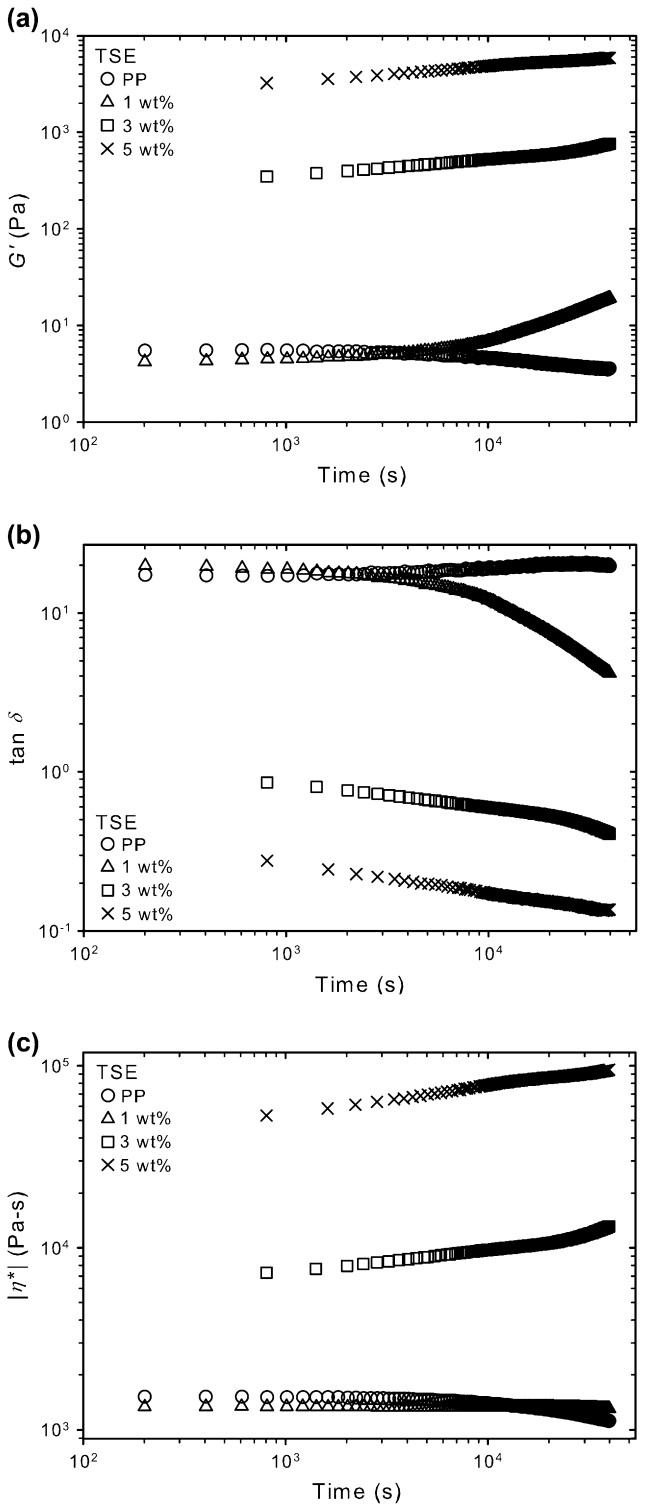


Fig. 6. Long-time SAOS of 1, 3, and 5 wt% TSE blends and processed PP performed for 11 h at 0.01 Hz, 200 °C, and 1% strain.

Increases in storage modulus and modest decreases in loss modulus for the three TSE blends contribute to concomitant decreases in the loss tangent. Finally, the results of the complex viscosity are initially puzzling, since the development of solid-like terminal rheology for the 1 wt% TSE sample does not translate to an increase in complex viscosity. However, it is important to recall that the loss modulus remains the dominant term in the calculation of the complex viscosity for that sample. With the loss modulus more than an order of magnitude larger than the storage modulus initially, a small percentage decrease in the former impacts the complex viscosity more significantly than a large percentage increase in the latter. Nevertheless, the decrease in complex viscosity associated with thermal degradation of the polymer is counterbalanced (1 wt% TSE) or overshadowed (3 and 5 wt% TSE) by the hypothesized changes in mesoscale organoclay structure that contribute to the increasingly solid-like rheology.

Before examining other samples, we first discuss the potential effect of surfactant degradation over the extended period of these long-time SAOS experiments. Research in other laboratories has shown that the 2M2HT surfactant used in the C15A organoclay begins to degrade at 200 °C, and thermogravimetric analysis confirms that approximately 27% of the surfactant originally present in the clay degrades over a period of 11 h at 200 °C. Surfactant degradation should lead to a decrease in mean basal spacing, as seen clearly in the XRD scans for the TSE (no PP-*g*-MA) sample in Fig. 2. However, at fixed organoclay loading, a decrease in basal spacing should *reduce* clay–clay interactions and result in *less* solid-like rheology. The fact that the opposite effect is observed indicates that surfactant degradation cannot explain the rheological data.

The appearance of signatures associated with the development of a mesoscale network in samples with organoclay loadings otherwise described by polymer-like rheology is a

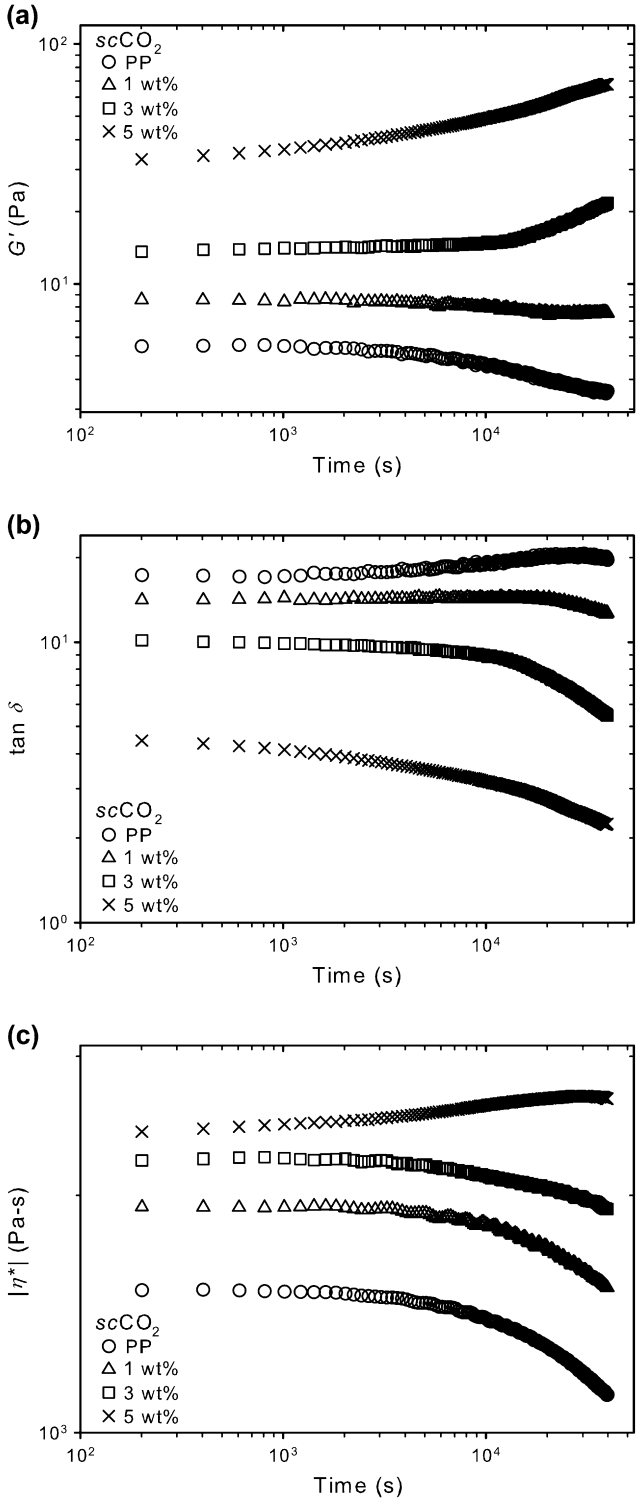


Fig. 7. Long-time SAOS of 1, 3, and 5 wt% $scCO_2$ blends and processed PP performed for 11 h at 0.01 Hz, 200 °C, and 1% strain.

surprising result. To further examine the relationship between exfoliation and loading on solid-like rheology, we present long-time SAOS data for the poorly exfoliated $scCO_2$ blends in Fig. 7. Although only the 5 wt% $scCO_2$ material shows any evidence of solid-like behavior in the frequency sweeps of Fig. 4, two-stage logarithmic time-dependence of the storage modulus is apparent for both 3 wt% ($\beta = 0.020$ and $\beta = 0.34$) and 5 wt% ($\beta = 0.097$ and $\beta = 0.26$) samples. Even at 1 wt%, the decrease in storage modulus due to thermal degradation is almost entirely offset by microstructural changes that hold the storage modulus to a modest 12% decline over the entirety of the experiment. For comparison, the storage modulus of the processed PP decreases by 35%. As expected, the time-dependent changes in the loss tangent and complex viscosity are muted relative to those for the TSE materials. In fact, of the $scCO_2$ blends, only the 5 wt% loading shows an increase in complex viscosity with time. Thus, we conclude that the long-time responses of the storage modulus and loss tangent are stronger indicators of mesoscale structural change, particularly at loadings below the ostensible mechanical percolation threshold. The loss modulus dominates the calculation of the complex viscosity in more polymer-like materials and masks the subtle microstructural evolution detected by the storage modulus and loss tangent. In summary, results for the poorly exfoliated $scCO_2$ blends indicate that mesoscale network formation occurs but its development is retarded when organoclay domains are initially more widely separated from one another.

According to Lee et al., time-dependent increases in the storage modulus may also be caused by intermolecular dipole–dipole and hydrogen-bonding associations between succinic anhydride and succinic acid (created by hydrolysis of succinic anhydride) functional groups pendant to PP-*g*-MA, which form a reversible, labile network [32]. A schematic of the hydrolysis process is shown in Fig. 8. To explore this possibility, we first present long-time SAOS rheological data for the TSE (no PP-*g*-MA) blends in Fig. 9, where the influence of organoclay on the development of solid-like rheology may be decoupled from that of the compatibilizer. Results for the storage modulus in Fig. 9(a) clearly show an overall

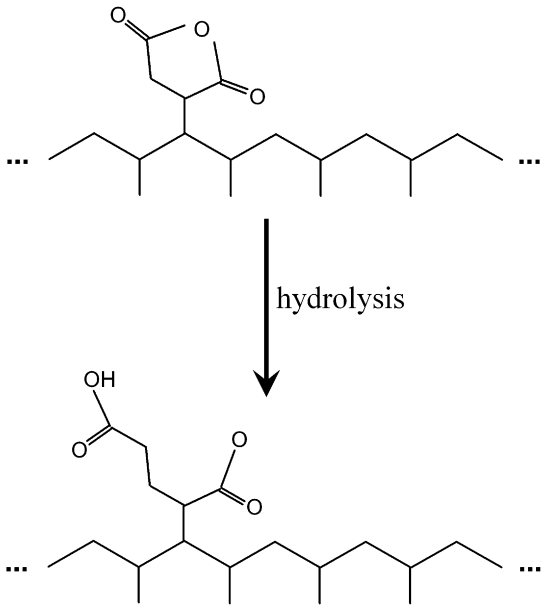


Fig. 8. Schematic of the hydrolysis of succinic anhydride groups pendant to PP-*g*-MA into succinic acid.

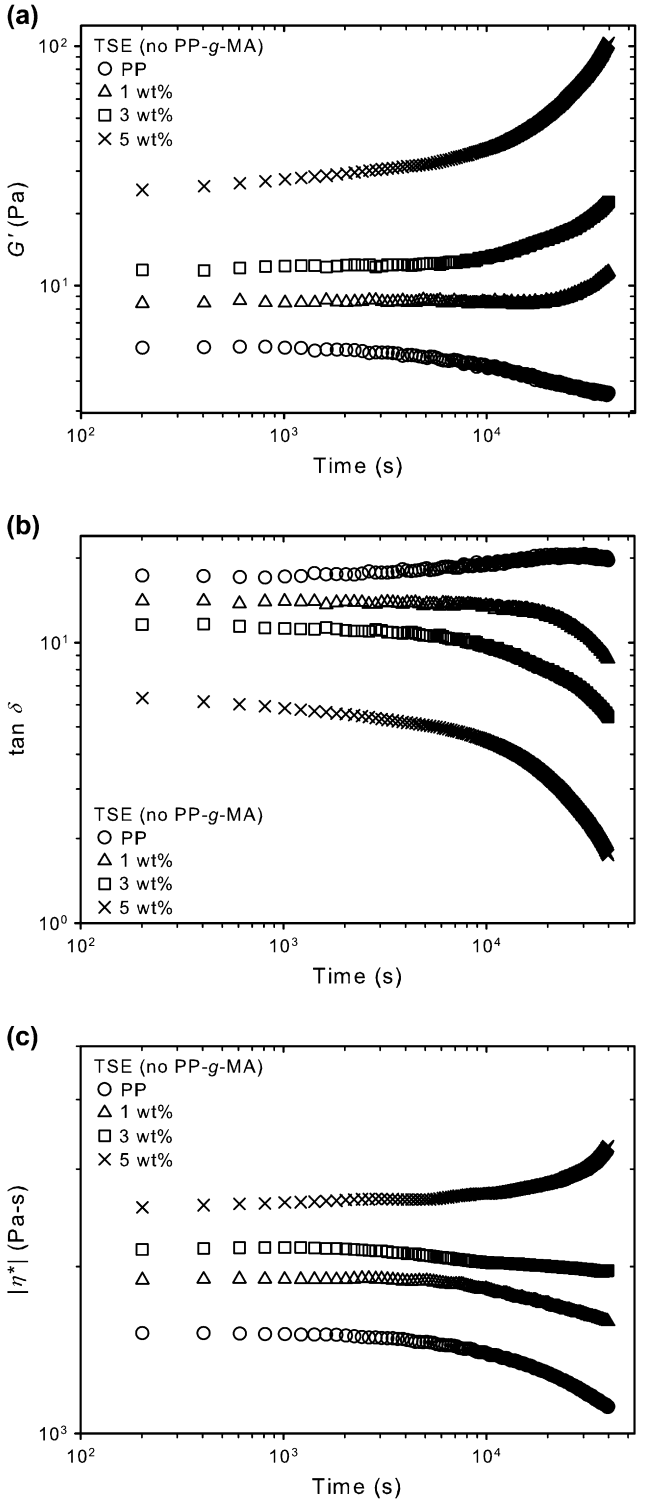


Fig. 9. Long-time SAOS of 1, 3, and 5 wt% TSE (no PP-*g*-MA) blends and processed PP performed for 11 h at 0.01 Hz, 200 °C, and 1% strain.

increase in storage modulus with annealing time at 1, 3, and 5 wt% organoclay loadings. Only the 5 wt% sample exhibits a clear two-stage time-dependence of the storage modulus ($\beta = 0.084$ and $\beta = 1.17$), as the storage modulus of the 1 and 3 wt% blends remains essentially flat for the first 1.25 and 5.25 h, respectively, before increasing with exponents of 0.56 and 0.61. The loss tangent data for the three TSE (no PP-*g*-MA) nanocomposites are qualitatively similar to those for the preceding two samples. Coupled with the storage modulus results, they demonstrate that organoclay plays a prominent role in the evolution of solid-like rheology with time.

Like the TSE and *sc*$CO_2$ materials, the complex viscosity results for TSE (no PP-*g*-MA) in Fig. 9(c) are less illustrative of the microstructural changes occurring in the fluid. Although the complex viscosity increases at 5 wt%, it decreases modestly with time for 1 and 3 wt%, though not as significantly as the processed PP. We also point out that the initial values of the complex viscosity are strikingly similar to those for the *sc*$CO_2$ samples despite the fact that the TSE (no PP-*g*-MA) blends are somewhat better exfoliated. However, the TSE (no PP-*g*-MA) materials have been subjected to higher stresses during melt blending and have suffered commensurately greater thermomechanical degradation. Thus, the initial complex viscosities of the TSE (no PP-*g*-MA) samples are only comparable to those of *sc*$CO_2$ due to improved exfoliation in TSE processing leading to greater clay–clay interactions.

The TSE (no PP-*g*-MA) results cannot eliminate the possibility that intermolecular associations between the pendant groups of the compatibilizer also contribute to a time-dependent increase in the storage modulus. To address this question, the PP/9 wt% PP-*g*-MA blend was subjected to the same long-time SAOS deformation history. The results of this test are shown in Fig. 10 and compared with the responses of processed PP and the three 3 wt% nanocomposites, two of which also contain 9 wt% compatibilizer. For the entire duration of the experiment, the rheological response of the PP/9 wt% PP-*g*-MA blend parallels that of the matrix PP, in contrast to the results reported by Lee et al. for pure PE-*g*-MA [32]. We posit that the reduced concentration of the maleated species is insufficient to form a volume-spanning physical network through intermolecular associations between succinic anhydride (and possibly succinic acid) pendant groups. Hence, the increasingly solid-like rheology observed in the 1 and 3 wt% blends stems solely from the presence of organoclay. Although it remains possible that PP-*g*-MA may form a physical network in the 5 wt% compatibilized samples (containing 15 wt% PP-*g*-MA), the strong influence of organoclay in the lower concentration samples suggests that the long-time rheology will continue to be dominated by clay–clay interactions.

Thus, we have shown that the inclusion of organoclay mediates the development of solid-like terminal rheology, while PP-*g*-MA (for the concentrations reported) does not contribute to the solid-like behavior other than to facilitate exfoliation and dispersion of the organoclay. While a definitive explanation of how organoclay influences the observed time-dependent terminal rheology remains elusive, the analogy to soft glassy dynamics, whereby the material resembles an attractive colloidal gel, remains the most plausible. Colloidal gels are characterized by an elastic, hierarchical, volume-spanning network that is heterogeneous on the length scale of the network [61]. Since long-range electrostatic repulsive interactions are not relevant in these materials, short-range attractive van der Waals forces are presumed to drive the formation of the

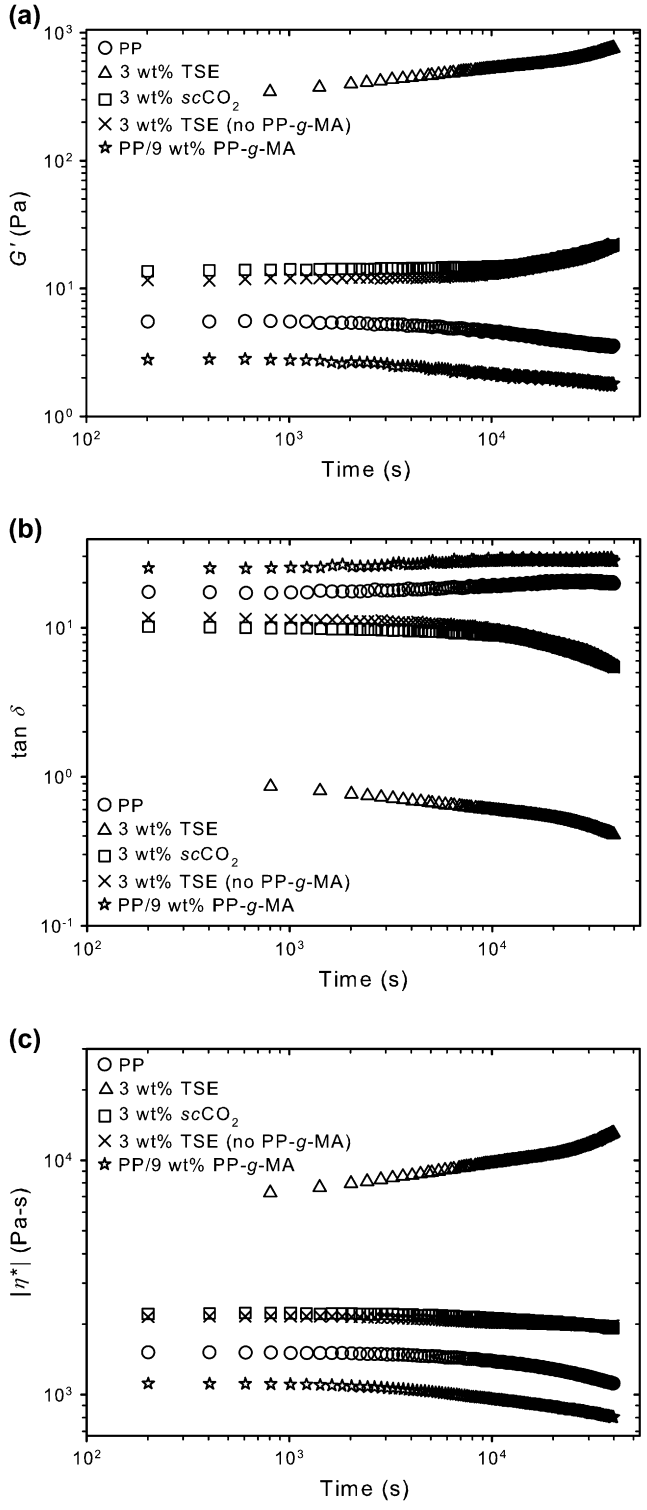


Fig. 10. Long-time SAOS of 3 wt% $scCO_2$, TSE, and TSE (no PP-*g*-MA) nanocomposites and processed PP and PP/9 wt% PP-*g*-MA performed for 11 h at 0.01 Hz, 200 °C, and 1% strain.

organoclay network. Importantly, because the network of a colloidal gel is heterogeneous, it is possible for a material to exhibit solid-like terminal rheology at organoclay loadings that otherwise lead to liquid-like rheology prior to network formation.

Before proceeding, it is vital to consider the role of compression molding on the observed rheological behavior. As mentioned earlier, samples were compression molded prior to experiments, a process that invariably drives a radial flow that could induce some preferred orientation of organoclay domains. One fundamental question is the mechanism by which organoclay disorientation occurs. Previously, we reported results for a single 3 wt% PP–clay nanocomposite, including an estimate of the rotational diffusivity due to Brownian motion of individual organoclay domains [31]. Because the time scale for rotational diffusivity exceeded that of the long-time SAOS experiments, we concluded that rotational Brownian motion did not drive organoclay disorientation. Solomon et al. reached the same conclusion in their work [24]. Furthermore, both studies further reinforce the notion that Brownian motion is unimportant by observing that the strain at which stress overshoots occurred during startup flow experiments was constant for all shear rates. Hence, it has been alternatively proposed that the same attractive van der Waals forces believed responsible for the formation of the mesoscale network also cause organoclay domains to disorient at short times during long-time SAOS.

Organoclay disorientation was further probed by contrasting long-time SAOS experiments on as-processed (but compression molded) and pre-sheared samples [31]. Independent of deformation history, the samples exhibited similar values of $\beta$ during the first 10,000 s of long-time SAOS. From this, one might infer that organoclay domains that are flow-aligned by compression molding or pre-shear disorient in the same fashion. On the other hand, startup flow experiments performed on the same samples suggest that other factors may be relevant, principally those derived from soft glassy dynamics. Specifically, the magnitude of the viscosity overshoot during startup from rest increased logarithmically with annealing time at a faster rate for as-processed samples. Had disorientation kinetics been the only important physics, the rate would have been independent of deformation history. Instead, the divergence of the as-processed and pre-sheared viscosity overshoot results suggests that the organoclay disorientation process may be arrested, perhaps due to the gradual formation of the mesoscale network. In that case, the individual organoclay domains that comprise the network are trapped in a metastable configuration from which they cannot escape, akin to the constitutive elements of colloidal glasses and gels. The second stage of the long-time SAOS experiments reported here, characterized by much higher values of $\beta$, may be indicative of a transition from organoclay domain disorientation to mesoscale network formation dictating the rheological response.

In summary, logarithmic increases in the storage modulus appear to be ubiquitous in PP–clay nanocomposites, independent of organoclay loading (within the range studied), degree of exfoliation, and compatibilization. In fact, the trend toward solid-like terminal rheology for samples that are ostensibly well below the threshold for mechanical percolation is remarkable. It reinforces the notion that van der Waals forces may drive network formation in these systems, where the resulting

volume-spanning, mesoscale network is highly heterogeneous on the length scale of the sample volume yet able to bear mechanical load. Further work focusing on the structure of the network is in progress.

## 4. Conclusions

An investigation into the origin of time-dependent terminal rheology in PP–clay nanocomposites was carried out. Nanocomposites containing 1, 3, and 5 wt% organoclay were prepared in the presence and absence of maleic anhydride functionalized PP compatibilizer using two melt-blending processes intended to induce varying degrees of clay silicate exfoliation. XRD scans show only modest differences in clay basal spacing, and the dependence of XRD results on sample preparation is demonstrated by comparing with samples annealed for 11 h. SAOS frequency sweep experiments differentiate between samples more clearly, as the terminal rheology is sensitive to organoclay loading and extent of exfoliation.

Continuous SAOS at fixed low frequency resolves a residual controversy as to whether the storage modulus increases or decreases with annealing time, as all samples exhibit logarithmically increasing storage modulus. Remarkably, even samples whose organoclay loading and degree of exfoliation place them below the threshold for mechanical percolation show increasingly solid-like terminal rheology during annealing. Such long-time behavior is also observed for samples that do not contain compatibilizer, affirming that the effect at least partially derives from the reorganization of organoclay domains. The logarithmic dependence of the storage modulus is consistent with the analogy to soft glassy dynamics espoused by Ren et al. [41]. Similar rheological experiments performed on a blend of PP and PP-*g*-MA reveal that the pendant group functionalities of the compatibilizer do not exhibit increasingly solid-like rheology over time, negating the likelihood that intermolecular associations between succinic anhydride and succinic acid contribute to the phenomenon.

## Acknowledgements

The authors thank Dr. Robert Sammler of The Dow Chemical Company for the generous donation of the H700-12 polypropylene resin, Dr. Leigh Allen of Crompton Corporation for the Polybond® 3200 PP-*g*-MA compatibilizer, and Dr. Doug Hunter of Southern Clay Products for the Cloisite® 15A montmorillonite clay. We are also grateful to Dr. Wei Zhang and Dr. Ronald D. Moffitt of the Advanced and Applied Polymer Processing Institute (AAPPI) for the use of the Leistritz Micro 27 twin-screw extruder and Prof. Donald G. Baird and graduate student Quang Nguyen in the Department of Chemical Engineering at the Virginia Polytechnic Institute and State University for permitting the use of the single-screw extruder with $sc CO_2$. Finally, we recognize the financial support of the National Science Foundation (NSF CAREER Award CTS-0134275).

## References

[1] Usuki A, Kawasumi M, Kojima Y, Okada A, Kurauchi T, Kamigaito O. J Mater Res 1993;8(5):1174–8.
[2] Usuki A, Kojima Y, Kawasumi M, Okada A, Fukushima Y, Kurauchi T, et al. J Mater Res 1993;8(5):1179–84.
[3] Kojima Y, Usuki A, Kawasumi M, Okada A, Fukushima Y, Kurauchi T, et al. J Mater Res 1993;8(5):1185–9.
[4] Lan T, Pinnavaia TJ. Chem Mater 1994;6(12):2216–9.
[5] Messersmith PB, Giannelis EP. J Polym Sci Part A Polym Chem 1995; 33(7):1047–57.
[6] Gilman JW, Jackson CL, Morgan AB, Harris R, Manias E, Giannelis EP, et al. Chem Mater 2000;12(7):1866–73.
[7] Alexandre M, Dubois P. Mater Sci Eng R 2000;28(1–2):1–63.
[8] Giannelis EP, Krishnamoorti R, Manias E. Adv Polym Sci 1999;138: 107–47.
[9] Ho DL, Briber RM, Glinka CJ. Chem Mater 2001;13(5):1923–31.
[10] Ray SS, Okamoto M. Prog Polym Sci 2003;28(11):1539–641.
[11] Marchant D, Jayaraman K. Ind Eng Chem Res 2002;41(25):6402–8.
[12] Wang Y, Chen FB, Li YC, Wu KC. Compos Part B Eng 2004;35(2): 111–24.
[13] Wang Y, Chen FB, Wu KC. J Appl Polym Sci 2004;93(1):100–12.
[14] Wang Y, Chen FB, Wu KC. Compos Interfaces 2005;12(3–4):341–63.
[15] Wang Y, Chen FB, Wu KC. J Appl Polym Sci 2005;97(4):1667–80.
[16] Wang Y, Chen FB, Wu KC, Wang JC. Polym Eng Sci 2006;46(3): 289–302.
[17] Bourbigot S, Vanderhart DL, Gilman JW, Awad WH, Davis RD, Morgan AB, et al. J Polym Sci Part B Polym Phys 2003;41(24):3188–213.
[18] Vaia RA, Liu WD, Koerner H. J Polym Sci Part B Polym Phys 2003; 41(24):3214–36.
[19] Treece MA, Oberhauser JP. J Appl Polym Sci 2007;103(2):884–92.
[20] Treece MA, Oberhauser JP. Polym Eng Sci, in press.
[21] Eckel DF, Balogh MP, Fasulo PD, Rodgers WR. J Appl Polym Sci 2004; 93(3):1110–7.
[22] Morgan AB, Gilman JW. J Appl Polym Sci 2003;87(8):1329–38.
[23] Khan SA, Prud'homme RK. Rev Chem Eng 1987;4(3–4):205–70.
[24] Solomon MJ, Almusallam AS, Seefeldt KF, Somwangthanaroj A, Varadan P. Macromolecules 2001;34(6):1864–72.
[25] Galgali G, Ramesh C, Lele A. Macromolecules 2001;34(4):852–8.
[26] Lele A, Mackley M, Galgali G, Ramesh C. J Rheol 2002;46(5): 1091–110.
[27] Koo CM, Kim MJ, Choi MH, Kim SO, Chung IJ. J Appl Polym Sci 2003; 88(6):1526–35.
[28] Li J, Zhou CX, Wang G, Zhao DL. J Appl Polym Sci 2003;89(13): 3609–17.
[29] Gu SY, Ren J, Wang QF. J Appl Polym Sci 2004;91(4):2427–34.
[30] Lertwilmolnun W, Vergnes B. Polymer 2005;46(10):3462–71.
[31] Treece MA, Oberhauser JP. Macromolecules 2007;40(3):571–82. doi: 10.1021/ma0612374.
[32] Lee JA, Kontopoulou M, Parent JS. Polymer 2004;45(19):6595–600.
[33] Kim YC, Lee SJ, Kim JC, Cho H. Polym J 2005;37(3):206–13.
[34] Mederic P, Razafinimaro T, Aubry T, Moan M, Klopffer MH. Macromol Symp 2005;221:75–84.
[35] Devendra R, Hatzikiriakos SG, Vogel R. J Rheol 2006;50(4):415–34.
[36] Krishnamoorti R, Giannelis EP. Macromolecules 1997;30(14):4097–102.
[37] Fornes TD, Yoon PJ, Keskkula H, Paul DR. Polymer 2001;42(25): 9929–40.
[38] Hoffmann B, Dietrich C, Thomann R, Friedrich C, Mulhaupt R. Macromol Rapid Commun 2000;21(1):57–61.
[39] Meincke O, Hoffmann B, Dietrich C, Friedrich C. Macromol Chem Phys 2003;204(5–6):823–30.
[40] Sohn JI, Lee CH, Lim ST, Kim TH, Choi HJ, Jhon MS. J Mater Sci 2003; 38(9):1849–52.
[41] Ren JX, Casanueva BF, Mitchell CA, Krishnamoorti R. Macromolecules 2003;36(11):4188–94.
[42] Zhao J, Morgan AB, Harris JD. Polymer 2005;46(20):8641–60.

[43] Maiti P. Langmuir 2003;19(13):5502–10.
[44] Ren JX, Silva AS, Krishnamoorti R. Macromolecules 2000;33(10): 3739–46.
[45] Mitchell CA, Krishnamoorti R. J Polym Sci Part B Polym Phys 2002; 40(14):1434–43.
[46] Ren JX, Krishnamoorti R. Macromolecules 2003;36(12):4443–51.
[47] Krishnamoorti R, Yurekli K. Curr Opin Colloid Interface Sci 2001; 6(5–6):464–70.
[48] Luckham PF, Rossi S. Adv Colloid Interface Sci 1999;82(1–3):43–92.
[49] Jogun SM, Zukoski CF. J Rheol 1999;43(4):847–71.
[50] Cocard S, Tassin JF, Nicolai T. J Rheol 2000;44(3):585–94.
[51] Willenbacher N. J Colloid Interface Sci 1996;182(2):501–10.
[52] Abou B, Bonn D, Meunier J. Phys Rev E 2001;64(2):021510.
[53] Bonn D, Tanase S, Abou B, Tanaka H, Meunier J. Phys Rev Lett 2002; 89(1):015701.
[54] Bellour M, Knaebel A, Harden JL, Lequeux F, Munch JP. Phys Rev E 2003;67(3):031405.
[55] Sollich P, Lequeux F, Hebraud P, Cates ME. Phys Rev Lett 1997;78(10): 2020–3.
[56] Fielding SM, Sollich P, Cates ME. J Rheol 2000;44(2):323–69.
[57] Cipelletti L, Ramos L. J Phys Condens Matter 2005;17(6):R253–85.
[58] Donth E. The glass transition: relaxation dynamics in liquids and disordered materials. Berlin: Springer-Verlag; 2001.
[59] Tanaka H, Meunier J, Bonn D. Phys Rev E 2004;69(3):031404.
[60] Tanaka H, Jabbari-Farouji S, Meunier J, Bonn D. Phys Rev E 2005;71(2): 021402.
[61] de Gennes PG. Scaling concepts in polymer physics. Ithaca: Cornell University Press; 1979.
[62] Wang YL, Ji DQ, Yang CL, Zhang HJ, Qin C, Huang BT. J Appl Polym Sci 1994;52(10):1411–7.
[63] Li G, Li H, Wang J, Park CB. In: Annual technical conference – Society of Plastics Engineers, vol. 63; 2005. p. 2332–6.
[64] Xie W, Gao Z, Pan W-P, Hunter D, Singh A, Vaia R. Chem Mater 2001; 13(9):2979–90.
[65] Gelfer M, Burger C, Fadeev A, Sics I, Chu B, Hsiao BS, et al. Langmuir 2004;20(9):3746–58.
[66] La Mantia FP, Dintcheva NT. Macromol Symp 2003;194:277–86.
[67] Machado AV, Maia JM, Canevarolo SV, Covas JA. J Appl Polym Sci 2004;91(4):2711–20.
[68] Berzin F, Vergnes B, Canevarolo SV, Machado AV, Covas JA. J Appl Polym Sci 2006;99(5):2082–90.
[69] Huang J-C, Xu J. Int J Polym Mater 2003;52(3):203–9.
[70] Lim YT, Park OO. Rheol Acta 2001;40(3):220–9.
[71] Lobe VM, White JL. Polym Eng Sci 1979;19(9):617–24.
[72] White JL, Tanaka H. J Appl Polym Sci 1981;26(2):579–89.
[73] Suetsugu Y, White JL. J Appl Polym Sci 1983;28(4):1481–501.
[74] Suh CH, White JL. J Non-Newtonian Fluid Mech 1996;62(2–3): 175–206.